



Exploring the antimalarial potential of the methoxy-thiazinoquinone scaffold: Identification of a new lead candidate

Concetta Imperatore^{a,1}, Marco Persico^{a,1}, Maria Senese^a, Anna Aiello^a, Marcello Casertano^a, Paolo Luciano^a, Nicoletta Basilico^{b,*}, Silvia Parapini^b, Antonella Paladino^c, Caterina Fattorusso^{a,*}, Marialuisa Menna^{a,*}

^a The NeaNat Group, Department of Pharmacy, University of Naples "Federico II", Via D. Montesano 49, 80131 Napoli, Italy

^b Dipartimento di Scienze Biomediche, Chirurgiche e Odontoiatriche, Università di Milano, Via Pascal 36, 20133 Milan, Italy

^c Istituto di Chimica del Riconoscimento Molecolare, CNR, Via M. Bianco 9, 20131 Milano, Italy

ARTICLE INFO

Keywords:

Organic synthesis
Thiazinoquinones
Antimalarial
DFT calculations
Reactive radical species
Redox-based mechanism of action

ABSTRACT

A small library of antiplasmodial methoxy-thiazinoquinones, rationally designed on the model of the previously identified hit **1**, has been prepared by a simple and inexpensive procedure. The synthetic derivatives have been subjected to *in vitro* pharmacological screening, including antiplasmodial and toxicity assays. These studies afforded a new lead candidate, compound **9**, endowed with higher antiplasmodial potency compared to **1**, a good selectivity index when tested against a panel of mammalian cells, no toxicity against RBCs, a synergistic antiplasmodial action in combination with dihydroartemisinin, and a promising inhibitory activity on stage V gametocyte growth. Computational studies provided useful insights into the structural requirements needed for the antiplasmodial activity of thiazinoquinone compounds and on their putative mechanism of action.

1. Introduction

According to the WHO World Malaria Report 2017 [1], in 2016 91 countries reported a total of 216 million cases of malaria, with an increase of 5 million cases over the previous year: actually, nearly half of the world's population is at risk of malaria [1,2]. Malaria deaths worldwide were 445 000 in 2016, approximately the same number as the previous year. Most of these cases were in the African Region (90%), followed by the South-East Asia Region (7%) and the Eastern Mediterranean Region (2%). *Plasmodium falciparum* (Pf) is the most prevalent malaria parasite in sub-Saharan Africa, accounting for 99% of estimated malaria cases in 2016 [1]. Great efforts have been made and are still being done in an attempt to eliminate malaria; however, a more attainable goal is controlling this disease.

A key role in the fight against malaria is played by the discovery of new drugs. Indeed, although today different types of antimalarial drugs are available and their use in combination is the best way to treat the

disease, nevertheless, new therapeutic agents are always needed to keep up with the evolution of parasite resistance [3]. In recent times we are witnessing a significant increase of new chemotypes active against *Plasmodium* but the challenge is now to assess their potential as anti-malarial leads. In this contest, the marine environment has played an important role in providing new chemical scaffolds [4]. In particular, a group of molecules isolated from marine invertebrates and characterized by the presence of a thiazinoquinone bicyclic moiety, showed interesting antiplasmodial properties [5,6]. This prompted us to explore the antiplasmodial potential of this scaffold, which is also contained in the structures of the aplidinones A and B (Fig. 1), two metabolites isolated by us from the Mediterranean ascidian *A. conicum* [7]. Accordingly, we decided to build a chemical library designed on the model of these simple natural thiazinoquinones [8,9]. A first series of synthetic derivatives were prepared and tested *in vitro* against both chloroquine (CQ)-sensitive (D10) and -resistant (W2) strains of Pf [8]. Many compounds showed interesting antiplasmodial activity, with IC₅₀

Abbreviations: Pf, *Plasmodium falciparum*; RBCs, red blood cells; SARs, structure-activity relationships; DFT, density functional theory; DHA, dihydroartemisinin; NAC, N-acetyl-L-cysteine; CAN, cerium ammonium nitrate; HMEC-1, human microvascular endothelial cells line 1; SI, selectivity index; BMDM, bone marrow-derived macrophages; THP-1, human monocytic leukaemia cells; MD, molecular dynamics; SA, Simulated annealing; MM, molecular mechanics; GM, global minimum; C-PCM, conductor-like polarizable continuum model; RMSD, root mean square deviation; LUMO, lowest unoccupied molecular orbital; NBO, natural bond orbitals; GSH, glutathione; iRBCs, infected red blood cells; ACT, artemisinin-based combination therapy

* Corresponding authors.

E-mail addresses: nicoletta.basilico@unimi.it (N. Basilico), cfattoru@unina.it (C. Fattorusso), mlmenna@unina.it (M. Menna).

¹ These authors contributed equally.

<https://doi.org/10.1016/j.bioorg.2018.12.031>

Received 13 August 2018; Received in revised form 19 December 2018; Accepted 22 December 2018

Available online 03 January 2019

0045-2068/ © 2019 Elsevier Inc. All rights reserved.

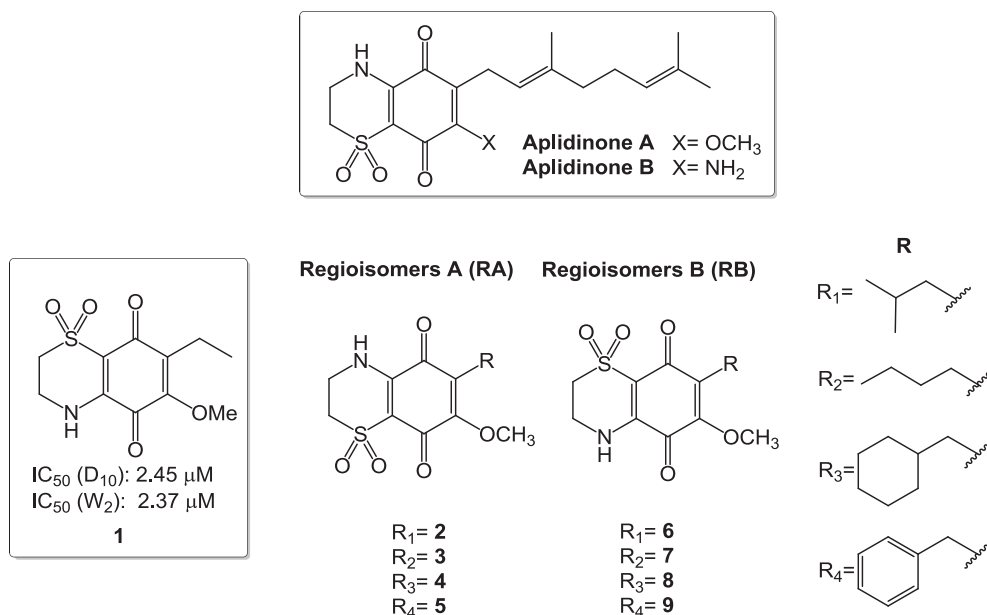


Fig. 1. Structures of Aplidinones A and B, of the thiazinoquinone-based starting hit (1), and of the new derivatives 2–9.

values in the low micromolar range [8]. Some of them were also strongly cytotoxic [9], as commonly found for thiazinoquinone compounds [10–13], but others had a good selectivity index with respect to normal human cells [8]. Structural requirements critical for both the antiparasmodial and the cytotoxic activity already appeared from these early studies: both the nature of the X group on the thiazinoquinone ring of aplidinones (Fig. 1) and its position with respect to the nitrogen or sulphur atom of the dioxothiazine ring, were shown to be crucial for compound potency. On the other hand, the length of the alkyl chain distinguished the antiparasmodial activity from the toxicity against normal human cells [8]. Structure-activity relationships (SARs) were investigated through computational and electrochemical studies and the capacity to produce a toxic semiquinone species able to form a stable adduct with Fe(III)-heme was found to be related to the antiparasmodial activity. As a whole, this first set of results confirmed the thiazinoquinone as a new and promising chemotype active against *Pf* and compound 1 (Fig. 1) was proposed as a new synthetic and low-cost antimalarial hit candidate [8].

In the present article, we report the optimization of the hit candidate 1, accomplished by the synthesis of a small and rationally designed series of new methoxy-thiazinoquinone derivatives, compounds 2–9 (Fig. 1).

Starting from the previously obtained results [8], our current aim was to investigate the role played on the antiparasmodial activity by both the regiochemistry of the methoxy-thiazinoquinone system and the nature of the side chain linked at the quinone ring. Thus, two set of regioisomers (RA and RB, Fig. 1) were prepared, all characterized by different R substituents (Fig. 1), rationally varied in shape and nature to expand 1 SARs. Through this approach we identified a new hit candidate, compound 9, endowed by higher antiparasmodial potency compared to 1 and a good (> 25) selectivity index when tested against a panel of mammalian cells.

Computational studies including density functional theory (DFT) calculations were performed on 2–9 in order to rationalize the observed SARs and shed light on the mechanism of action of this new promising class of antiparasmodial compounds. The new optimized hit 9 was subjected to further pharmacological characterization in order to explore its antimalarial potential. No haemolysis was observed at antiparasmodial doses, a synergistic antiparasmodial action in combination with dihydroartemisinin (DHA) was assessed, as well as, a promising low (< 15) micromolar activity on late-stage gametocytes. Experiments

in combination with N-acetyl-L-cysteine (NAC) were also performed to investigate 9 antiparasmodial mode of action. Both theoretical and experimental results support the hypothesis that the new optimized hit 9 is able to kill the parasite through the production of free radicals and the consequent induction of cellular oxidative stress.

2. Results and discussion

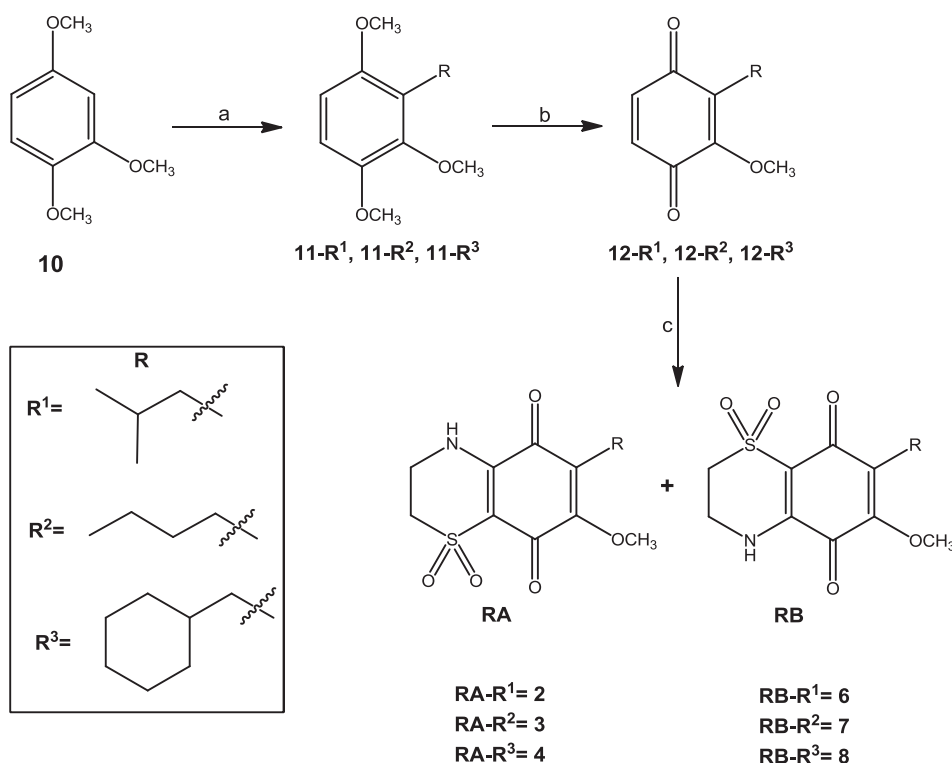
2.1. Synthesis

The methoxy-derivatives 2–4 and 6–8 were prepared using a synthetic approach similar to that adopted for the synthesis of compound 1 (Scheme 1) [8,9]. In the first step, the commercially available 1,2,4-trimethoxybenzene (10) was treated with *n*-BuLi in THF and, successively, with three different alkyl bromides, affording the corresponding 1,2,4-trimethoxy-3-alkylbenzenes 11-R¹, 11-R², and 11-R³ with good yields (80%, 76%, and 77%, respectively) [8].

The obtained methoxy alkyl benzenes 11-R¹, 11-R², and 11-R³ were oxidized with cerium ammonium nitrate (CAN) to give the quinones 12-R¹ (65% yield), 12-R² (65% yield), and 12-R³ (74% yield), respectively [14]. Subsequent reaction of each quinone with hypotaurine in the presence of catalytic amount of salcomine [15] allowed the thiazinoquinone bicyclic scaffold to be constructed. As previously observed for other unsymmetrical quinones [15,16], the biomimetic addition of hypotaurine to benzoquinones 12 afforded both thiazinoquinone regioisomers (RA and RB, Fig. 1) and was selective. Therefore, a mixture of 2 and 6 was obtained from 12-R¹, of 3 and 7 from 12-R², and of 4 and 8 from 12-R³, respectively. For all reactions, the outcome was highly (9:1) in favour of RB.

To prepare the benzyl-derivatives 5 and 9, the above synthetic scheme was slightly modified to increase the yields in the first step (Scheme 2). Therefore, after treatment of 1,2,4-trimethoxybenzene 10 with *n*-BuLi, benzaldehyde was added and the biaryl alcohol 13 was obtained. Compound 13 was then easily reduced by triethylsilane – trifluoroacetic acid in dichloromethane, and afforded compound 14 with very good yield [17,18]. Oxidation of 14 as described above (Scheme 1) gave the quinone 15 which, in turn, was subjected to condensation with hypotaurine in the presence of salcomine. Also in this case, a mixture of the isomeric (RA and RB) thiazinoquinones 5 and 9 was thus obtained in the ratio of 9:1 in favour of 9.

Each mixture of RA and RB (2/6, 3/7, 4/8, and 5/9) was easily



Scheme 1. Synthesis of compounds **2–4** and **6–8**^a. (^aReagents and conditions: (a) (1) *n*-BuLi, THF, 0 °C, 1 h; (2) **11-R¹**: 1-bromo-2-methylpropane, 0 °C → rt, 24 h. **11-R²**: 1-bromobutane, 0 °C → rt, 24 h. **11-R³**: bromomethylcyclohexane, 0 °C → rt, 24 h. (b) CAN, CH₃CN, 0 °C, 30 min. (c) hypotaurine, EtOH/CH₃CN, salcomine, rt, 24 h).

separated by HPLC into the individual components which were univocally distinguished and fully characterized by spectroscopic means (Tables S1 and S2).

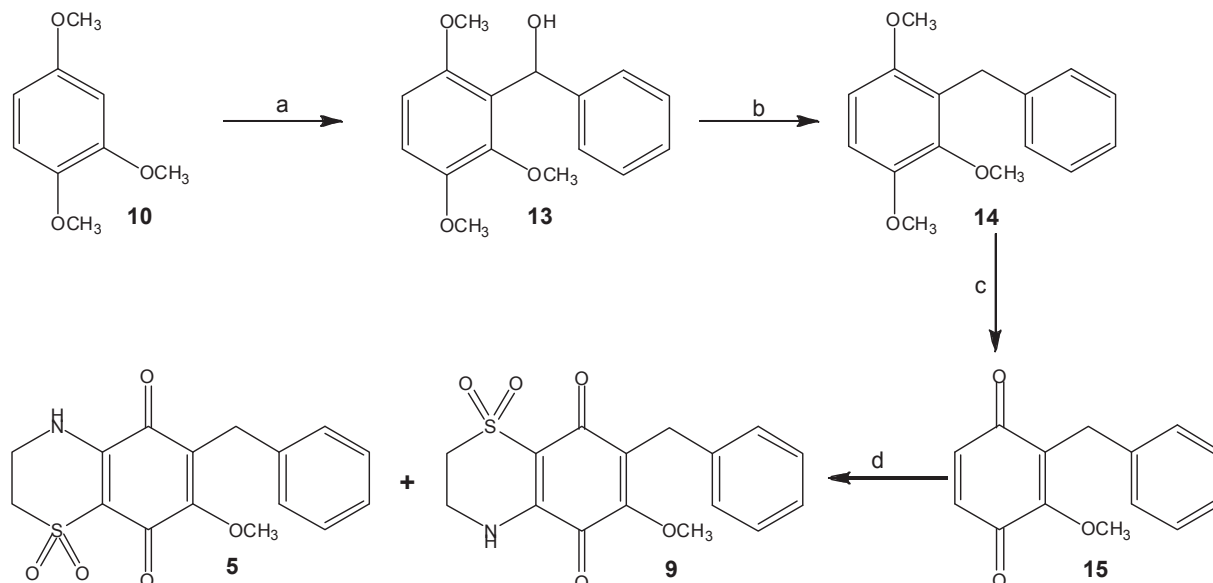
2.2. *In vitro* antimalarial activity and toxicity against human cells

Thiazinoquinones **2–9**, as well as the quinone intermediate **15**, were tested for their *in vitro* antiplasmodial activity against both chloroquine (CQ)-sensitive (D10) and CQ-resistant (W2) strains of *Pf*. Results are reported in Table 1.

All the RA (**2–5**), as well as compound **15**, showed an IC₅₀ higher than 10 μM. On the contrary, among the RB, **6–8** resulted active against

both strains, with IC₅₀ values in the low micromolar range, and **9** resulted active in the sub-micromolar range (Table 1). Thus, compound **9** resulted significantly more active than the identified starting hit **1**.

Then, we evaluated the cytotoxicity of the active regioisomers **6–9** against human microvascular endothelial cells (HMEC-1; Table 2). Only compound **8** showed cytotoxic activity in the low micromolar range. Among the new series of thiazinoquinones, compound **9** exhibited not only the highest antiplasmodial activity but also the higher selectivity index (SI = IC₅₀ on HMEC-1/IC₅₀ on *Pf* strains; Table 2). The selective toxicity of **9** was challenged also against other mammalian cell lines, such as, immortalized mouse C57Bl/6 bone marrow macrophages (BMDM) and human monocytic leukaemia cells (THP-1). Results



Scheme 2. Synthesis of compounds **5** and **9**. (^aReagents and conditions: (a) (1) *n*-BuLi, THF, 0 °C, 1 h; (2) benzaldehyde, 0 °C → rt, 12 h. (b) (1) TFA, CH₂Cl₂, rt, 10 min; (2) TES, rt, 12 h. (c) CAN, CH₃CN, 0 °C, 30 min. (d) hypotaurine, EtOH/CH₃CN, salcomine, rt, 24 h).

Table 1

clogD values and *in vitro* antiplasmodial activity of RA (2–5), RB (1 and 6–9), and compound 15 against CQ-sensitive (D10) and CQ-resistant (W2) *P. falciparum* strains.^a



Comp.	R	D10 IC ₅₀ (μM) ^b	W2 IC ₅₀ (μM) ^b	clogD ^c	Comp.	R	D10 IC ₅₀ (μM) ^b	W2 IC ₅₀ (μM) ^b	clogD ^c
RA-2	CH ₂ CH(CH ₃) ₃	> 10	> 10	-0.03	RB-6	CH ₂ CH(CH ₃) ₃	1.26 ± 0.21	2.82 ± 0.81	-0.03
RA-3	(CH ₂) ₃ CH ₃	> 10	> 10	0.15	RB-7	(CH ₂) ₃ CH ₃	1.75 ± 0.36	2.19 ± 0.57	0.15
RA-4	CH ₂ C ₆ H ₁₁	> 10	> 10	1.15	RB-8	CH ₂ C ₆ H ₁₁	2.37 ± 1.14	3.03 ± 1.14	1.15
RA-5	CH ₂ C ₆ H ₅	> 10	> 10	0.41	RB-9	CH ₂ C ₆ H ₅	0.60 ± 0.21	0.70 ± 0.22	0.41
15	CH ₂ C ₆ H ₅	> 10	> 10	2.67	1	CH ₂ CH ₃	2.45 ± 0.42	2.37 ± 0.42	-0.91

^a Chloroquine (CQ) has been used as positive control (D10 IC₅₀ = 0.04 ± 0.01; W2 IC₅₀ = 0.54 ± 0.28; not cytotoxic).

^b Data are the mean ± SD of three different experiments in duplicate.

^c clogD calculated considering pH values: 7.4, 7.2 and 5.5.

Table 2

IC₅₀ against HMEC-1, Selectivity Index (SI) and clogD values of the active compounds 1 and 6–9.

Comp.	IC ₅₀ (μM) ^a	SI ^b		clogD ^c
		D10	W2	
1	> 100	> 40.8	> 42.2	-0.91
6	26.8 ± 6.4	21.2	9.4	-0.03
7	40.2 ± 7.6	22.9	18.3	0.15
8	3.9 ± 0.1	1.6	1.3	1.15
9	17.6 ± 1.4	27.7	25.2	0.41

^a Data are the mean ± SD of three different experiments in duplicate.

^b SI = IC₅₀ mammalian cells/IC₅₀ *P. falciparum* strain.

^c logD calculated considering pH values: 7.4, 7.2 and 5.5.

confirmed a SI value > 25 (Table S3), as observed for the HMEC-1 cell line.

Based on these results, the newly identified antiplasmodial hit 9 was subjected to further *in vitro* pharmacological characterization (see the dedicated paragraph).

2.3. Structure-activity relationships (SARs) of the new thiazinoquinone derivatives

The whole of the antiplasmodial and cytotoxicity data allows making some important considerations. First, the *in vitro* effects on the parasite strains (Table 1) show that the antiplasmodial activity is not merely due to the presence of the redox-active 1,4-benzoquinone system. In fact, compound 15, analogue of the most active compound 9 but lacking the 1,1-dioxo-1,4-thiazine ring, resulted completely inactive, thus indicating the thiazinoquinone moiety as crucial for the antiplasmodial activity. In addition, among the tested thiazinoquinones, only RB, featuring the amine group at the same side of the methoxy group, showed significant antiplasmodial activity (Table 1). By consequence, not only the dioxothiazinoquinone ring system, but also a specific relative orientation of the quinone ring substituents, are required for the antiplasmodial activity.

Other interesting observations can be made based on the SARs of the active regioisomers 6–9, particularly considering the structural features differentiating the antiplasmodial from the cytotoxic activity. It has been reported for substituted 2-hydroxy-naphthoquinones (atovaquone analogues) that the inhibitory activity against the mitochondrial bc1 complex increases by increasing the length of the alkyl substituent, with a nine carbon atoms side-chain resulting the most effective one [19]. The same has been demonstrated for quinone-based compounds acting on *Pf*

alternative (Type II) NADH Dehydrogenases (complex I) [20]. In our case, the size of the alkyl substituent strongly influenced human cell cytotoxicity (1 vs. 7, 6 vs. 8; Table 2), while it has no significant effect on the antiplasmodial activity. This latter showed instead a significant improvement when a benzyl substituent was attached as R (compound 9; Table 1); on the contrary, HMEC-1 toxicity decreased when the cyclohexyl moiety of 8 was replaced by the aromatic ring of 9 (Table 2). Taken together our results suggest that, while the cytotoxic activity against human cells is possibly due to the action on the mitochondrial electron transport chain, for the antiplasmodial activity a different, but still redox-based, mechanism of action has to be evoked. Electrochemical studies previously performed on 1 as well as on other active and inactive analogues, evidenced that the antiplasmodial activity is related to the ability to produce a one-electron reduced semi-quinone species able to form a stable adduct with Fe(III)-heme, in which the metal is still redox-active [8]. On the other hand, previous biochemical results on thiazinoquinone-based natural compounds active against human cancer cells, demonstrated that their toxicity is due to the collapse of the mitochondrial membrane potential, in agreement with the currently observed SARs [10].

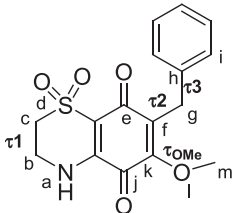
To take into account the role played by molecular pharmacokinetics on the observed SARs, distribution coefficient values of 1–9 were calculated (clogD, Tables 1 and 2) (ACD/Percepta 2017). RA and RB presented the same clogD values, indicating no influence of this parameter on the different antiplasmodial activity of the two sets of regioisomers. In addition, also within the series of the active RB analogues, no correlation was found between the clogD values and the antiplasmodial activity (Table 1). On the contrary, it emerged that a clogD value > 1 is required for cytotoxic activity against HMEC-1 cell (Table 2), in agreement with Lipinski's rules for drug absorption via passive diffusion [21]. Interestingly, the above results are similar to those previously obtained by us on a series of endoperoxide-based antimalarials [22], thus supporting the hypothesis that many antiplasmodial agents are actively transported into the infected erythrocyte by using the large number of membrane transport proteins expressed by the parasite on the host membrane [23].

2.4. Computational studies

To rationalize the observed SARs and gain new insight into the redox-based mechanism of action of our antiplasmodial thiazinoquinones, the steric and electronic features of the new series of compounds were investigated by mean of computational studies, including conformational analysis and DFT calculations.

Conformational analysis. The conformational space of compounds 2–9 and 15, was sampled by applying a calculation protocol including a

Table 3
 ΔE_{GM} values (kcal/mol) and torsion angle values (degrees) of the MM conformers of compound **9**.



Sub-family	ΔE_{GM} (kcal/mol) ^a	Torsion Angles (°) ^b			
		τ_{OMe} ^c	$\tau 1$ ^d	$\tau 2$ ^e	$\tau 3$ ^f
Ia	0.00–0.30	–39.20	58.44	95.56	–76.31
IIa	0.11–0.36	–40.43	–58.32	97.38	–74.61
Ib	0.11–0.36	40.43	58.32	–97.38	74.52
IIb	0.00–0.30	39.24	–58.44	–95.60	76.26

^a The values reported refer to the lowest and the highest energy conformers of the sub-family.

^b The values reported refer to the lowest energy conformer of the sub-family.

^c τ_{OMe} torsion angle is defined by j, k, l, and m atoms.

^d $\tau 1$ torsion angle is defined by a, b, c, and d atoms.

^e $\tau 2$ torsion angle is defined by e, f, g, and h atoms.

^f $\tau 3$ torsion angle is defined by f, g, h, and i atoms.

molecular dynamics (MD; simulated annealing (SA)) procedure combined with molecular mechanics (MM) energy minimization (see Experimental section for details). Then, all resulting conformers within 5 kcal/mol from the global minimum energy (GM) value were classified into families and sub-families according to the values of their torsion angles. In Table 3 are reported the results obtained for **9**, the most active compound of the series, while the complete set of results for compounds **2–8** and **15** is reported in Tables S4–S11 (Supporting Information). In Fig. 2 are reported the lowest energy conformers of all compounds superimposed by the quinone ring; the superimposition of all minima of all compounds is reported in Fig. S1.

Firstly, the conformers were grouped into two families, named I and II, according to the two thiazinoquinone ring flips, that is, having positive or negative value of $\tau 1$ (torsion angles defined as in Table 3 and Tables S4–S11), respectively ($\tau 1$ mean value = $\pm 63^\circ$; standard deviation = $\pm 5^\circ$).

All conformers presented (i) the same orientation of the methoxyl group (τ_{OMe} mean value = $\pm 36^\circ$; standard deviation = $\pm 5^\circ$), (ii) the rotation of the R substituent constrained by favourable electronic interactions occurring between the hydrogen atoms of the first methylene group and the oxygen atoms of, both, the quinone ring and the methoxyl group (intramolecular distance = 2.6 Å; Fig. 2).

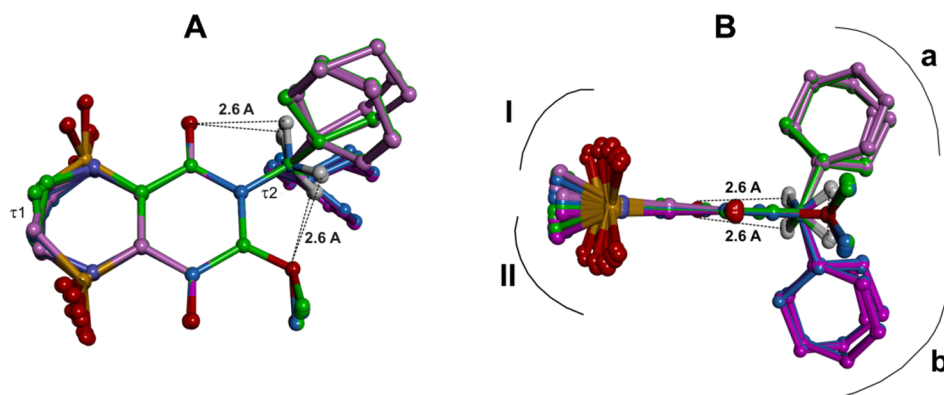


Fig. 2. (A) Top view and (B) transversal view of the lowest energy conformers of each sub-family of compounds **2–9** and **15** superimposed by e, f, k, and j atoms (for atom definition see Table 3). Carbon atoms are colored according to family classification (Ia = green, IIa = magenta, Ib = pink, and IIb = light blue); heteroatoms are colored by atom type (O = red, N = blue, S = yellow). Hydrogens are omitted for sake of clarity, with the exception of those of the first R methylene group, whose intramolecular distance from the oxygen atoms of the quinone and methoxyl groups are reported.

By consequence, the torsion angle $\tau 2$ showed just two possible values for each family ($\tau 2$ mean value = $\pm 91^\circ$; standard deviation of $\pm 9^\circ$), giving rise to two subsets of conformers (named a and b), for a total number of four sub-families: Ia ($\tau 1 + / \tau 2 +$), Ib ($\tau 1 + / \tau 2 -$), IIa ($\tau 1 - / \tau 2 +$), and IIb ($\tau 1 - / \tau 2 -$).

The two families presented isoenergetic minima, which resulted to be the mirror image of each other, namely, conformational enantiomers (Fig. S2, Supporting information). On the other hand, conformers belonging to the same subfamily slightly differed in the conformation of R, still presenting the same rotation of the first methylene group (i.e., the same value of $\tau 2$) and an overall similar volume occupation of the R substituent (Fig. S1). Going into details, the isopropyl moiety of **2** and **6** resulted to shift among three conformations for each sub-family ($\tau 3 = \sim 60^\circ$, $\sim -60^\circ$ and $\sim 180^\circ$; $\tau_{3GM} = \pm 56^\circ$; Tables S4 and S5) with a maximum contribution to the overall conformational energy of about 1.4 kcal/mol. Similarly, each sub-family of compounds **3** and **7** presented three possible values for the $\tau 3$ and $\tau 4$ torsion angles of the R butyl chain ($\sim 180^\circ$, $\sim 60^\circ$, and $\sim -60^\circ$; $\tau_{3GM} = \pm 179^\circ$; $\tau_{4GM} = \pm 180^\circ$; Tables S6 and S7), with a maximum contribution to the overall conformational energy of about 2.3 kcal/mol. On the other hand, the cyclohexyl ring of **4** and **8** assumed three orientations with respect to the thiazinoquinone ring ($\tau 3 = \sim 60^\circ$, $\sim -60^\circ$ and $\sim 180^\circ$; $\tau_{3GM} = \pm 56^\circ$; Tables S8 and S9) and the two chair conformations ($\tau 4 \sim 180^\circ$ and $\sim -80^\circ$; $\tau_{4GM} = \pm 180^\circ$; Tables S8 and S9). However, in this case, some conformers, such as, those with $\tau 3 \sim 180^\circ$ and $\tau 4 \sim -80^\circ$, are energetically disfavoured ($\Delta E_{GM} = 4.7$ kcal/mol) while all the others are grouped within an energy range of 2.3 kcal/mol.

Finally, in the case of compounds **5** and **9**, the phenyl ring assumed just one orientation in all sub-families, corresponding to a $\tau 3$ value of about -78° for family I and 78° for family II (standard deviation = $\pm 4^\circ$; Tables 3 and S10) with all the conformers within 0.34 kcal/mol from the GM.

In summary, our results evidenced that the new thiazinoquinone derivatives **2–9** show a limited energetically accessible conformational space (Figs. 2 and S1), characterized by (i) the presence of two specular sets of conformers having the opposite flip of the thiazinoquinone ring and (ii) a fixed orientation of the hydrogen atoms of the first methylene moiety of the R substituent (at 2.6 Å from either the closest quinone oxygen atom and the methoxy oxygen atom; Fig. 2), which restrained the conformational freedom of R, particularly in the derivatives **5** and **9** where the benzyl substituent presented just one conformation.

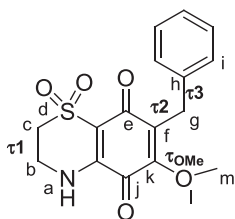
Importantly, the conformational behaviour resulted to be the same between the active (B) and inactive (A) regioisomers (Table 3, Tables S4–S11) evidencing that the different antiplasmodial activity is not due to their conformational features.

2.5. DFT calculations

In order to properly investigate the role of electronic properties on the antiplasmodial activity, DFT studies were performed on a selected

Table 4

ΔE_{GM} values (kcal/mol) and torsion angle values (degrees) of the DFT conformers of compound 9.



Sub-family	ΔE_{GM} (kcal/mol)	Torsion Angles (°)			
		τ_{OMe}^a	$\tau 1^b$	$\tau 2^c$	$\tau 3^d$
Ia	0.00	−61.99	60.22	93.27	−75.24
IIa	0.16	−62.43	−60.32	97.69	−67.94
Ib	0.16	62.43	60.32	−97.69	67.94
IIb	0.00	62.01	−60.23	−93.25	75.21

^a τ_{OMe} torsion angle is calculated considering j, k, l, and m atoms.

^b $\tau 1$ torsion angle is defined by a, b, c, and d atoms.

^c $\tau 2$ torsion angle is calculated considering e, f, g, and h atoms.

^d $\tau 3$ torsion angle is calculated considering f, g, h, and i atoms.

subset of compounds. In particular, calculations were performed on: (i) the most active compound 9 (D10 IC_{50} = 0.6 μ M, W2 IC_{50} = 0.7 μ M), presenting a benzyl substituent as R, (ii) its inactive regioisomer 5, (iii) compound 4 (not active) and (iv) 8 (D10 IC_{50} = 2.4 μ M, W2 IC_{50} = 3.0 μ M), that is, the couple of regioisomers presenting a cyclohexylmethyl substituent as R, and, finally, (v) compound 15 (not active), lacking the dioxothiazine ring. In order to mimic an aqueous environment, all DFT calculations were performed using the conductor-like polarizable continuum model (C-PCM) [24] as solvent model. Moreover, to characterize every structure as minimum, a vibrational analysis was carried out (see the Experimental Section for details).

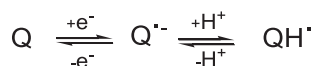
Fully optimized DFT conformers were classified into families and sub-families as previously described for the MM conformers (Tables 4 and S12–S15).

As can be inferred by comparing the data in Table 3 with those in Table 4, after DFT optimization, the structures of the neutral quinone species conserved their overall conformational features (root mean square deviation (RMSD) mean value on all atoms: 0.2830 Å; Fig. S3) and energy classification (Tables S12–S15).

The mechanism of action of antimalarial quinones is ascribed to their redox properties, and, in particular, the antiplasmodial activity of quinone-based compounds has been related to their semi-quinone form [8]. Accordingly, starting from the lowest energy conformer of each subfamily, we considered the one-electron reduction pathway of the thiazinoquinone scaffold in protic solvents (Scheme 3).

According to the frontier orbital theory, the energy of the lowest unoccupied molecular orbital (LUMO) accounts for the propensity of the molecule to acquire an electron while its location allows to identify the most probable site to be reduced (i.e., to accept the electron). Hence, we analysed the energy and the location of the LUMO in all the DFT minima. The results evidenced a relationship between the observed antiplasmodial activity and, both, electron affinity (Table 5) and the LUMO position in the quinone species (Fig. 3).

Firstly, the rank of the calculated LUMO energy values (Table 5) reflected the antiplasmodial activity (Table 1). Indeed, compounds 8 and 9 presented significantly lower LUMO energy with respect to the



Scheme 3. Quinone one-electron reduction pathway in protic solvents.

Table 5

Calculated energy values (kcal/mol) of the LUMO of compounds 4, 8, 5, 9, and 15.

Comp.	4	8	5	9	15
E_{LUMO}	−14.27	−19.74	−15.53	−20.49	−13.60

corresponding inactive regioisomers 4 and 5, and compound 15 (inactive), which lacks the 1,1-dioxo-1,4-thiazine ring, showed the highest LUMO energy value.

Then, in the active regioisomers 8 and 9 the LUMO is localized on the quinone carbonyl function adjacent to the methoxyl substituent while in the inactive regioisomers 4 and 5 it is placed on the quinone carbonyl function adjacent to the R substituent (Fig. 3, B, D vs A, C). Thus, the propensity of the compound to be firstly reduced on one quinone carbonyl function rather than the other resulted a crucial issue for antiplasmodial activity. Interestingly, in the studied compounds such propensity is not dependent on the nature of the R substituent but on the regiochemistry of the thiazinoquinone system, favouring the carbonyl function close to the NH group.

Starting from the DFT conformers of the parent quinones, the next step was to generate the corresponding semiquinone radicals and submit them to full DFT optimization. After DFT calculations, the semiquinone species of the active regioisomers 8 and 9 presented the oxygen atom of the methoxyl group involved in a hydrogen bond with the newly generated hydroxyl group (Fig. 4B and S4B).

The unpaired electron spin density of the semi-quinone species was calculated by using the natural bond orbitals (NBO) population analysis [25]. It resulted that the radical is differently delocalized on the two regioisomers (Figs. 4 and S4, A vs B). Importantly, the DFT results also allowed to hypothesize the possible redox-based mechanism of action of the active thiazinoquinones. Indeed, in the active regioisomers 8 and 9, a “through space” hydrogen radical could be shifted from a carbon atom of the R substituent to the carbonyl oxygen atom (Fig. 5).

The putative hydrogen radical shift would lead to the reduction to hydroquinone, accompanied by the formation of a carbon radical on the R substituent. In support to this hypothesis, the above reported conformational analysis results showed that all low energy conformers present a hydrogen of the first methylene group of R placed at 2.6 Å from the quinone oxygen, a distance suitable for an intra-molecular hydrogen radical shift. In the semi-quinone form of 9 this distance is shortened to 2.45 Å (Fig. 4B), in this compound the hydrogen radical shift would be favoured by the formation of a benzyl radical (10) and this could account for its higher antiplasmodial activity with respect to the other analogues in which R is an aliphatic substituent.

On these bases, we propose that thiazinoquinones, upon interaction with the redox partner, give rise to an oxygen-centered radical. Then, an intramolecular radical shift to a carbon atom of the side chain R occurs that leads to the putative toxic species for the *Plasmodium* environment.

Heme metabolism represents a well-known antimalarial target [26] and the one-electron reduction of the natural endoperoxide drug artemisinin by free heme has been reported to be the key bio-activation step leading to the toxic radical species [27]. As above mentioned, previous cyclovoltammetry studies [8] evidenced that the thiazinoquinone derivatives showing antiplasmodial activity towards D10 and W2 strains (< 10 μ M), produced a redox-active adduct between their semi-quinone form and free heme, and that the stability of such adduct was related to their antiplasmodial potency. On the contrary, in the same conditions, the inactive analogues underwent a two-electron reduction/oxidation cycle without any interaction with the free heme present in solution. Accordingly, to complete our investigation, we performed a fragment-based search in the Cambridge Crystallographic Structural Database (software Conquest 1.19; Cambridge Structural Database System 2016) to investigate which functional group of the methoxy-thiazinoquinone

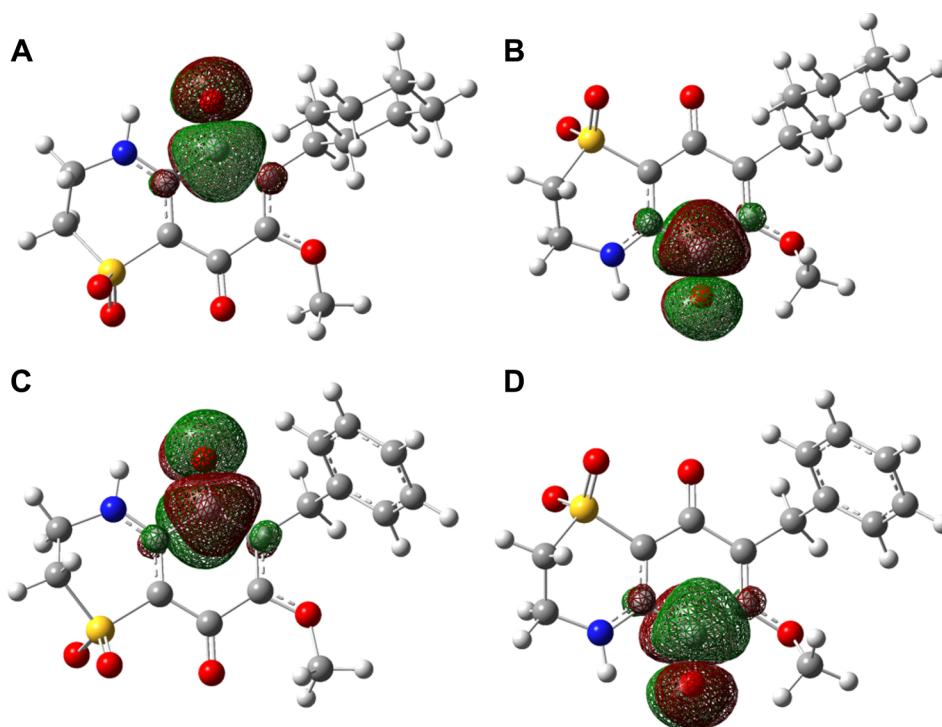


Fig. 3. Localization of the lowest unoccupied molecular orbital (LUMO) of **4** (A), **8** (B), **5** (C), and **9** (D). The ligands are displayed in ball&stick and colored by atom type (C = gray, O = red, N = blue, S = yellow and H = white). The orbitals were visualized using GaussView with an isosurface value of $0.02 e^-/a.u.^3$.

system could be suitable for iron interaction (for details see experimental section). In summary, the analysis of 192 identified hits evidenced that only the oxygen atoms of the quinone and methoxyl functions were found to coordinate iron in X-ray determined complexes (Fig. 6). On the contrary, the SO_2 function alone or adjacent to a quinone oxygen were not found to complex iron.

Taken together, our results suggested that (i) the 1,1-dioxo-1,4-thiazine ring fused to the quinone ring, as well as, the regiochemistry of the resulting thiazinoquinone system, play a key role in the electron affinity of the compounds, (ii) the quinone oxygen near the amine function is likely the first to be reduced, being involved in the first step of the putative bio-activation reaction (i.e., one-electron reduction reaction), (iii) the positioning of the hydrogen atoms of the first methylene group of the R substituent with respect to the semi-quinone oxygen radical is critical for the observed antiplasmodial activity since it may favour a hydrogen radical shift from the carbon to the oxygen atom generating a toxic radical species able to impair the *Pf* antioxidant defences, (iv) the nature of substituent R affects the antiplasmodial potency according to the stability of the putative carbon radical, and (v)

the methoxyl group favours the interaction with the redox partner (i.e., heme) without interfering with the redox reaction.

3. *In vitro* pharmacological characterization of compound **9**

3.1. Effect of *N*-acetyl-L-cysteine (NAC) on the antiplasmodial activity

To support the hypothesis that the mechanism of action of our antiplasmodial thiazinoquinones was related to the generation of toxic free radicals, compound **9** was tested against *Pf* infected red blood cells (RBCs) pre-treated with increasing doses of the free radical scavenger NAC. As shown in Table 6, the antiplasmodial activity of compound **9** was dose dependently decreased (i.e., the IC_{50} was increased) by different doses of NAC. NAC is a well-known antioxidant which stimulates the synthesis of glutathione (GSH) [28]. Pre-treatment of infected RBC with NAC might lead to an increase of reduced GSH preventing the accumulation of free radicals. For example, the antiplasmodial activity of artesunate, which is known to induce free radicals formation, is also reduced by NAC [29].

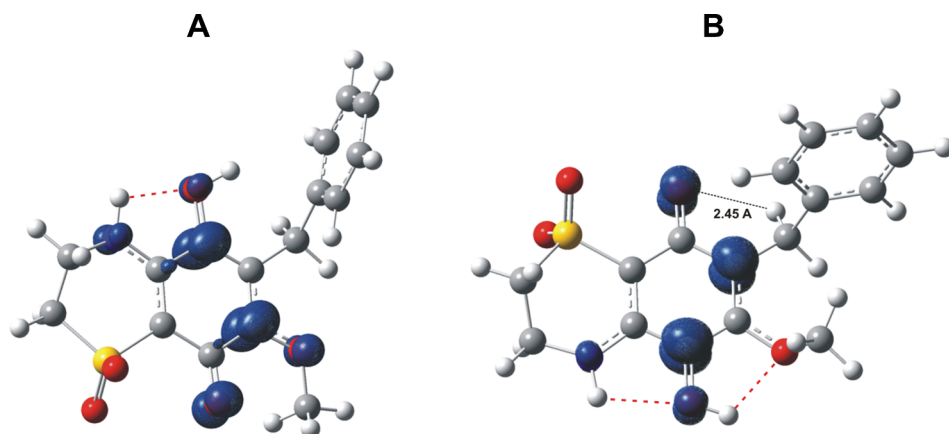


Fig. 4. NBO spin density isosurface of QH^\bullet species of **5** (A) and **9** (B). The spin density was visualized using GaussView with an isosurface value of $0.01 e^-/a.u.^3$. The blue surface (positive spin density) corresponds to an excess of α -electron density. The intramolecular distance between the methylene hydrogen of R and the oxygen atom of the quinone is reported. Hydrogen bonds are highlighted by a red dashed line. The ligands are displayed in ball&stick and colored by atom type (C = gray, O = red, N = blue, S = yellow and H = white).

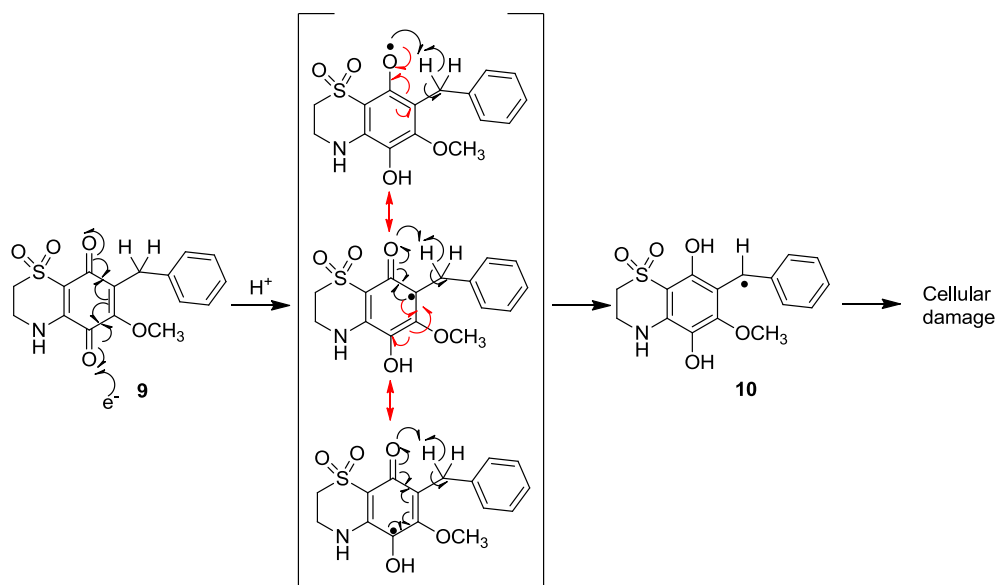


Fig. 5. Proposed mechanism for the formation of the putative toxic free radical (10) through generation of a semi-quinone species of 9 (red arrows indicate electron delocalization) followed by intramolecular hydrogen radical shift.

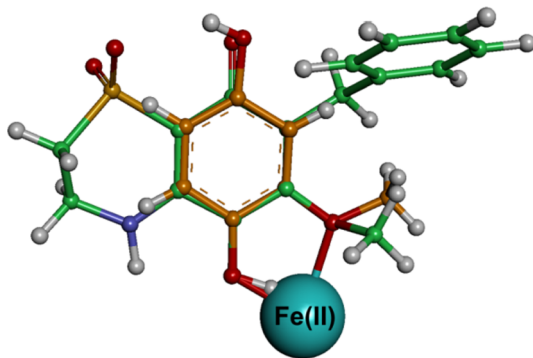


Fig. 6. QH[•] species of 9 (green) superimposed on the X-ray structure of 2-methoxyhydroquinonate in complex with iron (orange; CSD code: EPIMIB). The superimposition was made fitting the iron coordinating groups. vdW volume of iron atom (cyan) is scaled (0.5) for clarity. Heteroatoms are colored: O, red; N, blue; Fe, magenta; and Cl, light green.

Table 6

In vitro antiplasmodial activity of compound 9 against *P. falciparum*, W2 (CQ-R) strain, pretreated with increasing concentration of N-acetyl-L-cysteine (NAC).

Comp.	W2 (CQ-R)			
	- IC ₅₀ (μM) ^a	NAC 0.1 IC ₅₀ (μM) ^a	NAC 1 IC ₅₀ (μM) ^a	NAC 10 IC ₅₀ (μM) ^a
9	0.7 ± 0.2	0.7 ± 0.2	1.0 ± 0.2	1.3 ± 0.3

^a Data are the mean and SD of three experiments in duplicate.

3.2. Red blood cells (RBCs) toxicity

The formation of methaemoglobin, which can be generated by oxidative stress, was evaluated in RBCs treated with different doses of compound 9. The formation of methaemoglobin could be indicative of possible toxicity on RBCs. However, methaemoglobin was formed only at doses of compound 9 higher than the IC₅₀ on asexual parasite, indicating that the active doses were not toxic.

The experiment was carried out using the algorithm of Winterbourn [30] and was performed in the complete medium used for parasite growth in the presence or not of NAC. Similar experiments were carried

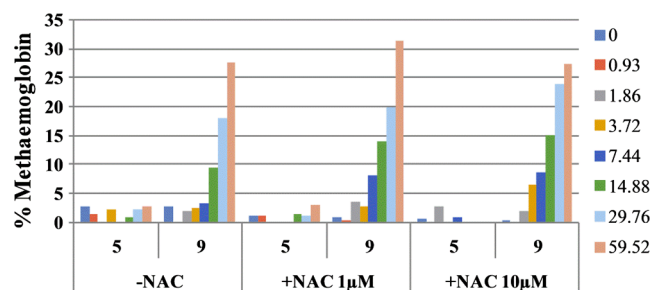


Fig. 7. Percentage of methaemoglobin formation after 24 h treatment of RBC with different doses of compounds 5 or compound 9. RBC were left in medium or pretreated with increasing concentration of NAC for 3 h and then incubated with compound 5 or 9 for further 24 h. Methaemoglobin formation was then determined. Data are from a representative experiment in triplicate.

out on compound 5, the inactive regioisomer of 9. As shown in Fig. 7, the levels of methaemoglobin in control RBCs were less than 1%, as reported for normal RBCs [31]. Compound 5 did not induce methaemoglobin formation at any of the doses used, whereas 9 increased the % of methaemoglobin formation at doses higher than 7.4 μM, but no more than 30% methaemoglobin at the highest concentration. To verify the ability of NAC to protect from methaemoglobin formation, the experiments were conducted pretreating RBCs with NAC. Differently from what observed for the activity of compound 9 on the parasite, NAC was not able to protect from methaemoglobin formation induced by compound 9. These results clearly indicate that only the active thiazinoquinone is able to oxidize haemoglobin, however only at higher concentration and, contrarily to what observed for the antiplasmodial activity, the presence of NAC did not affect methaemoglobin formation.

To further exclude a direct toxic effect of compounds 5 and 9 on RBCs, haemolysis was measured in uninfected and infected RBCs (iRBCs) treated with the compounds. No appreciable haemolytic activity of either uninfected or infected RBCs was observed compared to untreated controls with compounds 5 and 9 even at very high concentration (Fig. 8).

3.3. Combination with dihydroartemisinin (DHA)

Experiments were conducted to investigate a possible application of compound 9 in an artemisinin-based combination therapy (ACT).

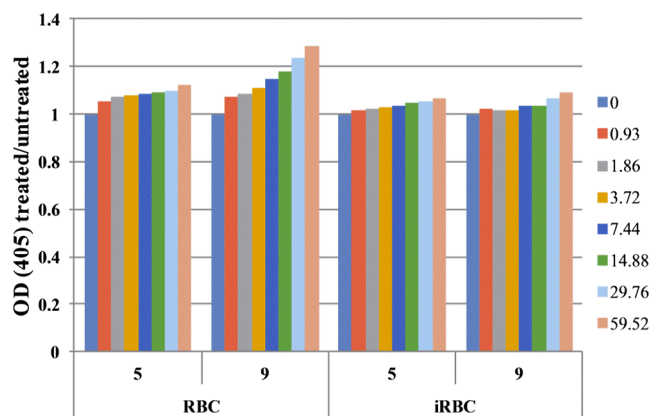


Fig. 8. Haemolytic effect of compounds 5 and 9, evaluated as release of haemoglobin in the supernatants (OD405). RBC or iRBC were incubated for 24 h with different concentration of compound 5 or 9. The histogram represents the ratio between the OD treated versus untreated RBC or iRBC. Data are from a representative experiment in triplicate.

Commonly, studies on drug combinations are performed in order to identify synergistic interactions to reduce the doses of the drugs, and, consequently, the side effects, maintaining the therapeutic efficacy. In the case of antimalarial drugs, combination therapies are used both to improve drug efficacy, and to delay the development of resistance to the individual components of the combination by reducing the selection of drug-resistant parasites.

The *in vitro* interaction of 9 with DHA was analysed by the use of isobolograms. Compound 9 was applied alone or in combination with DHA to W2 strain of *Pf*. In addition, a dose-response curve of DHA alone was performed to obtain the DHA IC_{50} . When tested in combination, five fixed doses of DHA (from 0.002 to 0.8 nM) were added to the dose-response curve of compound 9 (from 0.075 to 5 μ M). The isobologram was, then, constructed by plotting a pair of fractional IC_{50} s (IC_{50} of the drug in combination/ IC_{50} of the drug alone) for each combination of compound 9 with DHA (Fig. 9).

An isobologram close to the diagonal indicates an additive effect, curves above or below the diagonal indicate antagonistic or synergistic effect, respectively. The isobologram obtained for compound 9 provides a graphical representation of a synergistic interaction of this compound with DHA against W2 strain. This underlies a synergistic mechanism of action through which the combined drugs cooperate in killing the parasite [32]. Our results can be explained taking into account that artemisinin, as other endoperoxide-based antimalarials, are reported to be bioactivated via the reduction of the dioxane function, likely by heme or ferrous iron, thereby producing toxic free radicals which induce oxidative stress within the parasite [27,33,34]. Thus, according to

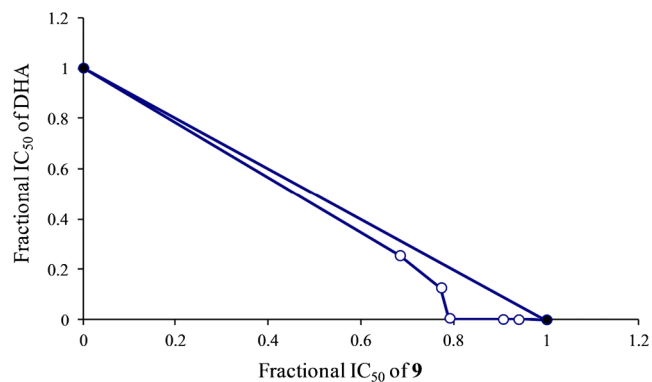


Fig. 9. Isobologram of the interaction between different doses of compound 9 and DHA on W2 strain of *P. falciparum*. The data are the mean of three independent experiments.

the postulated redox-based mechanism of action of our thiazinoquinones, it is not surprising that the *in vitro* antimalarial activity of DHA is enhanced by addition of another free radical generating compound, such as 9 [27,33,34].

3.4. Activity on late stage gametocytes

Eradicating malaria will require medicines that prevent transmission of the parasite between humans and mosquitoes. The goal to prevent *Pf* transmission from humans to mosquitoes requires the identification of a molecular target in mature (IV–V) stage gametocytes, the sexual stages circulating in the bloodstream. To investigate the transmission blocking potential of the methoxy-thiazinoquinone scaffold, compound 9 was tested against V stage *Pf* gametocytes. An IC_{50} of $13.8 \pm 5.6 \mu$ M was obtained, indicative of a lower activity against the sexual blood parasite stage with respect to the asexual stage. Nevertheless, this represented an encouraging result since, while some antimalarial drugs are active against immature (I–III) stage gametocytes, targeting mature (IV–V) stage gametocytes is currently problematic as they are refractory to most antimalarial drugs, with the exception of primaquine. DHA itself induces a 40% of mature gametocytes growth inhibition only at 10 μ M [35]. Even a drug in clinical development with activity against gametocytes, such as OZ277, has been shown to have *in vitro* activity against stage V gametocytes with an IC_{50} of 6.4 μ M [35,36].

4. Conclusions

Starting from the previously identified hit candidate 1, a small and rationally designed series of new antiplasmodial methoxy-thiazinoquinone derivatives has been developed. In particular, the role played on the activity by both the regiochemistry of the methoxy-thiazinoquinone system and the nature of the side chain linked at the quinone ring has been explored. These studies afforded a new hit candidate, compound 9, endowed with higher antiplasmodial potency compared to 1, no toxicity against RBCs, a good (> 25) selectivity index when tested against a panel of mammalian cells, and a promising inhibitory activity on stage V gametocyte growth. A synergistic antiplasmodial action in combination with DHA was evidenced, too. At the same time, computational studies shed light on the putative mechanism of action of antiplasmodial thiazinoquinones. In particular, it emerged that the regiochemistry of the thiazinoquinone system plays a key role both in the electron affinity of the compounds and in determining the first site to be reduced in the putative bio-activation step. Then, in the active RB, the positioning of the hydrogen atoms of the first methylene of the R alkyl group with respect to the semi-quinone oxygen radical represents a key issue which could favour a hydrogen radical shift and form a toxic carbon radical species able to impair the *Pf* antioxidant defences. In this view, the higher antiplasmodial potency of 9 reflects the stability of the benzyl radical formed after the putative radical shift.

5. Experimental section

5.1. General methods

Commercial reagents: Sigma–Aldrich. Solvents: Carlo Erba. TLC: Silica Gel 60 F254 (plates 5×20 , 0.25 mm) Merck. Preparative TLC: Silica Gel 60 F254 plates (20×20 , 2 mm). Spots revealed by UV lamp then by spraying with 2N sulfuric acid and heating at 120 °C. Anhydrous solvents: Sigma–Aldrich or prepared by distillation according to standard procedures. High-resolution ESI-MS analyses were performed on a Thermo LTQ Orbitrap XL mass spectrometer (Thermo-Fisher, San José, CA, USA). The spectra were recorded by infusion into the ESI (Thermo-Fisher, San José, CA, USA) source dissolving the sample in MeOH. 1H (700 MHz) and ^{13}C (175 MHz) NMR spectra were recorded on a Agilent INOVA spectrometer (Agilent Technology,

Cernusco sul Naviglio, Italy) equipped with a ^{13}C enhanced HCN Cold Probe; chemical shifts were referenced to the residual solvent signal (CDCl_3 ; $\delta_{\text{H}} = 7.26$, $\delta_{\text{C}} = 77.0$; $\text{DMSO}-d_6$ $\delta_{\text{H}} = 2.39$, $\delta_{\text{C}} = 39.0$). For an accurate measurement of the coupling constants, the one-dimensional ^1H NMR spectra were transformed at 64 K points (digital resolution: 0.09 Hz). Homonuclear ($^1\text{H}-^1\text{H}$) and heteronuclear ($^1\text{H}-^{13}\text{C}$) connectivities were determined by COSY and HSQC experiments, respectively. Two and three bond $^1\text{H}-^{13}\text{C}$ connectivities were determined by gradient 2D HMBC experiments optimized for a 2,3J of 8 Hz. $^3J_{\text{H-H}}$ values were extracted from 1D ^1H NMR. High performance liquid chromatography (HPLC) separations were achieved on a Shimadzu LC-10AT (Shimadzu, Milan, Italy) apparatus equipped with a Knauer K-2301 (LabService Analytica s.r.l., Anzola dell'Emilia, Italy) refractive index.

5.2. Syntheses

5.2.1. 2-isobutyl-1,3,4-trimethoxybenzene (**11-R¹**), 2-butyl-1,3,4-trimethoxybenzene (**11-R²**) and 2-(cyclohexylmethyl)-1,3,4-trimethoxybenzene (**11-R³**)

1.68 g (10 mmol) of 1,2,4-trimethoxybenzene (**10**) were dissolved in 25 mL of anhydrous THF and 12.5 mL of a *n*-BuLi 1.6 M solution (20 mmol) were added, under argon atmosphere at 0 °C; the mixture was stirred for 1 h. Then, 20 mmol of 1-bromo-2-methylpropane (2.2 mL), 1-bromobutane (2.1 mL), or bromomethylcyclohexane (2.8 mL) were added and the mixture was left under stirring for 24 h (the end of the reaction was controlled with TLC, eluent: chloroform/hexane = 7:3). After this time, the mixture was poured into cold water (150 mL) and extracted three times with diethyl ether. The ethereal solution was washed with brine several times, dried over sodium sulfate, filtered and concentrated under reduced pressure. The residue was purified by column chromatography on silica gel (hexane/EtOAc = 9:1) to afford **11-R¹** (1.8 g, 80.3% yield), **11-R²** (1.7 g, 76.0% yield) and **11-R³** (2.0 g, 76.5% yield) as colorless oil. **11-R¹**: ^1H NMR (CDCl_3): 6.68 (^1H , d, $J = 8.8$ Hz, H-6); 6.51 (1H, d, $J = 8.8$ Hz, H-5); 3.79 (3H, s, -OCH₃); 3.78 (3H, s, -OCH₃); 3.73 (3H, s, -OCH₃); 2.49 (2H, d, $J = 7.3$ Hz, CH₂); 1.89 (1H, m, $J = 7.3$ Hz-6.7 Hz, CH); 0.86 (6H, d, $J = 6.7$ Hz, CH₃); HRMS (ESI): m/z [$\text{M} + \text{Na}^+$]⁺ calcd. for $\text{C}_{13}\text{H}_{20}\text{O}_3\text{Na}^+$: 247.1305, found: 247.1314. **11-R²**: ^1H NMR (CDCl_3): 6.69 (^1H , d, $J = 8.8$ Hz, H-6); 6.52 (1H, d, $J = 8.8$ Hz, H-5); 3.77 (3H, s, -OCH₃); 3.74 (3H, s, -OCH₃); 3.72 (3H, s, -OCH₃); 2.63 (2H, t, $J = 7.4$ Hz, CH₂CH₂CH₂CH₃); 1.49 (2H, m, CH₂CH₂CH₂CH₃); 1.38 (2H, m, CH₂CH₂CH₂CH₃); 0.92 (3H, d, $J = 6.7$ Hz, CH₃); HRMS (ESI): m/z [$\text{M} + \text{Na}^+$]⁺ calcd. for $\text{C}_{13}\text{H}_{20}\text{O}_3\text{Na}^+$: 247.1305, found: 247.1315. **11-R³**: ^1H NMR (CDCl_3): 6.69 (^1H , d, $J = 8.8$ Hz, H-6); 6.52 (1H, d, $J = 8.8$ Hz, H-5); 3.80 (3H, s, -OCH₃); 3.78 (3H, s, -OCH₃); 3.74 (3H, s, -OCH₃); 2.50 (2H, d, $J = 7.4$ Hz, CH₂-cyclohexyl); 1.55 (1H, m, CH); 1.53–0.95 (4H, m); 1.15–1.66 (4H, m), 1.60 (2H, m); HRMS (ESI): m/z [$\text{M} + \text{Na}^+$]⁺ calcd. for $\text{C}_{16}\text{H}_{24}\text{O}_3\text{Na}^+$: 287.1618, found: 287.1626.

5.2.2. 2-isobutyl-3-methoxycyclohexa-2,5-diene-1,4-dione (**12-R¹**), 2-butyl-3-methoxycyclohexa-2,5-diene-1,4-dione (**12-R²**), 2-(cyclohexylmethyl)-3-methoxycyclohexa-2,5-diene-1,4-dione (**12-R³**)

3.5 mmol of each compound **11R¹⁻³** (780 mg of **11-R¹**, 780 mg of **11-R²**, 925 mg of **11-R³**) dissolved in 90 mL of acetonitrile were added dropwise to a solution of CAN (9.6 g, 17.5 mmol) in water (100 mL) at 0 °C. The mixture was stirred for 30 min at room temperature (the end of the reaction was checked by TLC, eluent: chloroform/EtOAc = 7:3). The orange liquid was then poured into 100 mL of cold water and extracted three times with diethyl ether. The combined organic layers were washed with brine, dried over sodium sulfate, and filtered. The solvent removal under reduced pressure afforded **12-R¹** (445 mg, 65%), **12-R²** (445 mg, 65%), and **12-R³** (610 mg, 74%) sufficiently pure for the following reaction. **12-R¹**: ^1H NMR (CDCl_3): 6.66 (^1H , d, $J = 10.0$ Hz, H-6); 6.51 (1H, d, $J = 10.0$ Hz, H-5); 3.99 (3H, s, -OCH₃); 2.34 (2H, d, $J = 7.3$ Hz, CH₂); 1.81 (1H, m, $J = 7.3$ Hz-6.7 Hz, CH); 0.89 (6H, d, $J = 6.7$ Hz, CH₃); HRMS (ESI): m/z [$\text{M} + \text{Na}^+$]⁺ calcd. for

$\text{C}_{11}\text{H}_{14}\text{O}_3\text{Na}^+$: 217.0835, found: 217.0841. (**12-R²**): ^1H NMR (CDCl_3): 6.66 (^1H , d, $J = 10.0$ Hz, H-6); 6.51 (1H, d, $J = 10.0$ Hz, H-5); 4.01 (3H, s, -OCH₃); 2.42 (2H, t, $J = 7.4$ Hz, CH₂CH₂CH₂CH₃); 1.47 (2H, m, CH₂CH₂CH₂CH₃); 1.39 (2H, m, CH₂CH₂CH₂CH₃); 0.92 (3H, d, $J = 6.7$ Hz, CH₃); HRMS (ESI): m/z [$\text{M} + \text{Na}^+$]⁺ calcd. for $\text{C}_{11}\text{H}_{14}\text{O}_3\text{Na}^+$: 217.0835, found: 217.0843. (**12-R³**): ^1H NMR (CDCl_3): 6.69 (^1H , d, $J = 8.8$ Hz, H-6); 6.52 (1H, d, $J = 8.8$ Hz, H-5); 4.01 (3H, s, -OCH₃); 2.35 (2H, d, $J = 7.4$ Hz, CH₂-cyclohexyl); 1.55 (1H, m, CH); 1.53–0.95 (4H, m); 1.15–1.66 (4H, m), 1.60 (2H, m); HRMS (ESI): m/z [$\text{M} + \text{Na}^+$]⁺ calcd. for $\text{C}_{14}\text{H}_{18}\text{O}_3\text{Na}^+$: 257.1148, found: 257.1139.

5.2.3. Condensation of quinones **12R¹⁻³** with hypotaurine

1.5 mmol of each quinone **12R¹⁻³** (290 mg of **12-R¹**, 290 mg of **12-R²**, 350 mg of **12-R³**) were dissolved in a mixture of EtOH/CH₃CN = 1: 1 and heated in a water bath under stirring; then, a solution of hypotaurine (163.7 mg, 1.5 mmol) in 8 mL of water and a catalytic amount of salcomine were added in portions. The mixture was stirred for 24 h at room temperature and the yellow solution became orange/red. Most of the ethanol was removed in vacuo and the residue was poured into water. The mixture was extracted with diethyl ether (three times) and the organic phase was washed with brine, dried over sodium sulfate, and filtered. Solvent removal gave residues containing mixtures of compounds **2/6** (from **12-R¹**, 170 mg, 38% yield), **3/7** (from **12-R²**, 173 mg, 39% yield) as well as of compounds **4/8** (from **12-R³**, 167 mg, 33% yield); they were separated as reported below.

5.2.4. Separation of crude mixtures of **2/6**, **3/7** and **4/8** isomers

Separation of isomers **2** and **6** mixture (170 mg) was achieved by HPLC on a SiO₂ column (Luna 5 μm, 250 × 4.60 mm) eluting with EtOAc/hexane 6:4 (v/v) and afforded pure compounds **2** (8 mg) and **6** (70 mg). Mixture of isomers **3** and **7** (170 mg), as well as that of **4** and **8** (167 mg), were separated in the same conditions and yielded pure compounds **3** (7 mg), **7** (67 mg), **4** (5 mg), and **8** (49 mg).

5.2.5. 6-isobutyl-7-methoxy-3,4-dihydro-2H-benzo[*b*][1,4]thiazine-5,8-dione 1,1-dioxide (**2**)

HPLC EtOAc/hexane 6:4 (v/v), (t_{R}): 13.5 min (single peak). ^1H and ^{13}C NMR data are reported in Tables S1 and S2. HRMS (ESI): m/z [$\text{M} + \text{Na}^+$]⁺ calcd. for $\text{C}_{13}\text{H}_{17}\text{NO}_5\text{SNa}^+$: 322.0720, found: 322.0727.

5.2.6. 7-isobutyl-6-methoxy-3,4-dihydro-2H-benzo[*b*][1,4]thiazine-5,8-dione 1,1-dioxide (**6**)

HPLC EtOAc/hexane 6:4 (v/v), (t_{R}): 24 min (single peak). ^1H and ^{13}C NMR data are reported in Tables S1 and S2. HRMS (ESI): m/z [$\text{M} + \text{Na}^+$]⁺ calcd. for $\text{C}_{13}\text{H}_{17}\text{NO}_5\text{SNa}^+$: 322.0720, found: 322.0729.

5.2.7. 6-butyl-7-methoxy-3,4-dihydro-2H-benzo[*b*][1,4]thiazine-5,8-dione 1,1-dioxide (**3**)

HPLC EtOAc/hexane 6:4 (v/v), (t_{R}): 11.5 min (single peak). ^1H and ^{13}C NMR data are reported in Tables S1 and S2. HRMS (ESI): m/z [$\text{M} + \text{Na}^+$]⁺ calcd. for $\text{C}_{13}\text{H}_{17}\text{NO}_5\text{SNa}^+$: 322.0720, found: 322.0733.

5.2.8. 7-butyl-6-methoxy-3,4-dihydro-2H-benzo[*b*][1,4]thiazine-5,8-dione 1,1-dioxide (**7**)

HPLC EtOAc/hexane 6:4 (v/v), (t_{R}): 22 min (single peak). ^1H and ^{13}C NMR data are reported in Tables S1 and S2. HRMS (ESI): m/z [$\text{M} + \text{Na}^+$]⁺ calcd. for $\text{C}_{13}\text{H}_{17}\text{NO}_5\text{SNa}^+$: 322.0720, found: 322.0735.

5.2.9. 6-(cyclohexylmethyl)-7-methoxy-3,4-dihydro-2H-benzo[*b*][1,4]thiazine-5,8-dione 1,1-dioxide (**4**)

HPLC EtOAc/hexane 6:4 (v/v), (t_{R}): 11.8 min (single peak). ^1H and ^{13}C NMR data are reported in Tables S1 and S2. HRMS (ESI): m/z [$\text{M} + \text{Na}^+$]⁺ calcd. for $\text{C}_{16}\text{H}_{21}\text{NO}_5\text{SNa}^+$: 362.1033, found: 362.1042.

5.2.10. 7-(cyclohexylmethyl)-6-methoxy-3,4-dihydro-2H-benzo[b][1,4]thiazine-5,8-dione 1,1-dioxide (8)

HPLC EtOAc/hexane 6:4 (v/v), (t_R): 21.4 min (single peak). ^1H and ^{13}C NMR data are reported in Tables S1 and S2. HRMS (ESI): m/z [$\text{M} + \text{Na}^+$] $^+$ calcd. for $\text{C}_{16}\text{H}_{21}\text{NO}_5\text{SNa}^+$: 362.1033, found: 362.1038.

5.2.11. phenyl(2,3,6-trimethoxyphenyl)methanol (13)

To a solution of 1,2,4-trimethoxybenzene (1.0 mL, 6.7 mmol) in THF (25 mL) was added 6 mL *n*-BuLi 1.6 M solution (10 mmol) under argon atmosphere at 0 °C; the mixture was stirred for 1 h. Then, the benzaldehyde (1.0 mL, 10 mmol) was added and the mixture was left under stirring at room temperature overnight and quenched with saturated NH_4Cl solution (30 mL). The two layers were separated and the aqueous layer was extracted with ether (three times). The combined organic layers were washed with brine, dried over anhydrous sodium sulfate, and concentrated in vacuo. The crude material was purified by column chromatography on silica gel (hexane/EtOAc = 8:2) to afford the corresponding biaryl alcohol **13** (1.3 g, 70% yield): ^1H NMR (CDCl_3): 6.82 (1H, d, J = 8.8 Hz, H-6); 6.62 (1H, d, J = 8.8 Hz, H-5); 3.82 (3H, s, $-\text{OCH}_3$); 3.74 (3H, s, $-\text{OCH}_3$); 3.61 (3H, s, $-\text{OCH}_3$); 6.25 (1H, d, J = 11.7 Hz, CH-OH); 7.36 (2H, d, J = 7.0 Hz); 7.28 (2H, t, J = 7.6 Hz); 7.19 (1H, t, J = 7.6 Hz); 4.29 (1H, d, J = 11.7 Hz, OH). HRMS (ESI): m/z [$\text{M} + \text{Na}^+$] $^+$ calcd. for $\text{C}_{16}\text{H}_{18}\text{O}_4\text{Na}^+$: 297.1097, found: 297.1109.

5.2.12. 2-benzyl-1,3,4-trimethoxybenzene (14)

Trifluoroacetic acid (0.5 mL, 7.2 mmol) was slowly added to a solution of phenyl(2,3,6-trimethoxyphenyl)methanol (**13**) (650 mg, 2.4 mmol) and triethylsilane (1.1 mL, 7.2 mmol) in dichloromethane (30 mL). The mixture was stirred at room temperature overnight. The organic phase was washed with a sodium carbonate solution (30 mL) and dried. The solvent removal afforded **14** (570 mg, 93%) sufficiently pure for the following reaction. ^1H NMR (CDCl_3): 6.73 (1H, d, J = 8.8 Hz, H-6); 6.56 (1H, d, J = 8.8 Hz, H-5); 3.80 (3H, s, $-\text{OCH}_3$); 3.72 (3H, s, $-\text{OCH}_3$); 3.68 (3H, s, $-\text{OCH}_3$); 4.01 (1H, s, CH_2 -benzyl); 7.22 (2H, d, J = 7.0 Hz); 7.18 (2H, t, J = 7.6 Hz); 7.09 (1H, t, J = 7.6 Hz). HRMS (ESI): m/z [$\text{M} + \text{Na}^+$] $^+$ calcd. for $\text{C}_{16}\text{H}_{18}\text{O}_3\text{Na}^+$: 281.1148, found: 281.1154.

5.2.13. 2-benzyl-3-methoxycyclohexa-2,5-diene-1,4-dione (15)

502 mg (2.2 mmol) of **14** dissolved in 90 mL of acetonitrile were added dropwise to a solution of CAN (6.0 g, 11.0 mmol) in water (110 mL) at 0 °C. The mixture was stirred for 30 min at 0 °C (the end of the reaction was checked by TLC, eluent: chloroform/EtOAc = 7:3). The orange liquid was then poured into 100 mL of cold water and extracted three times with diethyl ether. The combined organic layers were washed with brine, dried over sodium sulfate, and filtered. The solvent removal under reduced pressure afforded 324 mg of **15** (65%), sufficiently pure for the following reaction. ^1H NMR (CDCl_3): 6.66 (1H, d, J = 10.0 Hz, H-6); 6.57 (1H, d, J = 10.0 Hz, H-5); 4.02 (3H, s, $-\text{OCH}_3$); 3.77 (1H, s, CH_2 -benzyl); 7.25 (2H, d, J = 7.0 Hz); 7.23 (2H, t, J = 7.6 Hz); 7.16 (1H, t, J = 7.6 Hz). HRMS (ESI): m/z [$\text{M} + \text{Na}^+$] $^+$ calcd. for $\text{C}_{14}\text{H}_{12}\text{O}_3\text{Na}^+$: 251.0679, found: 251.0689.

5.2.14. Condensation of quinone 15 with hypotaourine

324 mg (1.42 mmol) of quinone **15** was dissolved in 26 mL of a mixture of EtOH/ CH_3CN 1:1 and heated in a water bath under stirring; then, a solution of hypotaourine (155 mg, 1.42 mmol) in 2 mL of water and a catalytic amount of salcomine were added in portions. The mixture was stirred for 24 h at room temperature (the end of the reaction was checked by TLC, eluent: chloroform: EtOAc = 7:3). The yellow solution became orange/red. Most of the ethanol was removed in vacuo and the residue was poured into water. The mixture was extracted with diethyl ether (three times) and the organic phase was washed with brine, dried over sodium sulfate, and filtered. Solvent removal gave residues containing a mixture of the isomers **5** and **9** (175 mg, 37%) which was separated as reported below.

5.2.15. Separation of crude mixtures of 5 and 9 isomers

Separation of isomers **5** and **9** mixtures (175 mg) was achieved by HPLC on a SiO_2 column (Luna 5 μm , 250×4.60 mm) eluting with EtOAc/hexane = 6:4 (v/v) and afforded pure compounds **5** (7 mg) and **9** (63 mg).

5.2.16. 6-benzyl-7-methoxy-3,4-dihydro-2H-benzo[b][1,4]thiazine-5,8-dione 1,1-dioxide (5)

HPLC EtOAc/hexane 6:4 (v/v), (t_R): 14 min (single peak). ^1H and ^{13}C NMR data are reported in Tables S1 and S2. HRMS (ESI): m/z [$\text{M} + \text{Na}^+$] $^+$ calcd. for $\text{C}_{16}\text{H}_{15}\text{NO}_5\text{SNa}^+$: 356.0563, found: 356.0565.

5.2.17. 7-benzyl-6-methoxy-3,4-dihydro-2H-benzo[b][1,4]thiazine-5,8-dione 1,1-dioxide (9)

HPLC EtOAc/hexane 6:4 (v/v), (t_R): 27 min (single peak). ^1H and ^{13}C NMR data are reported in Tables S1 and S2. HRMS (ESI): m/z [$\text{M} + \text{Na}^+$] $^+$ calcd. for $\text{C}_{16}\text{H}_{15}\text{NO}_5\text{SNa}^+$: 356.0563, found: 356.0565.

5.3. Parasite growth and drug susceptibility assay

Unless stated otherwise all reagents were from Sigma Italia, Milan, Italy.

The CQ sensitive (D10) and the CQ resistant (W2) strains of *Pf* were maintained *in vitro* as described [37] at 5% hematocrit (human type A-positive red blood cells) in RPMI 1640 (EuroClone, Celbio) medium with the addition of 1% AlbuMax (Invitrogen, Milan, Italy), 0.01% hypoxanthine, 20 mM HEPES, and 2 mM glutamine. Cultures were maintained at 37 °C in a standard gas mixture of 1% O_2 , 5% CO_2 , and 94% N_2 . Compounds were dissolved in DMSO and then diluted with medium to achieve the required concentrations (final DMSO concentration < 1%, which is nontoxic to the parasite). Drugs were placed in 96 well flat-bottom microplates and serial dilutions made. Asynchronous cultures (parasitemia of 1–1.5%; 1% final hematocrit) were aliquoted into the plates and incubated for 72 h at 37 °C. In some experiments, the W2 strain culture was pretreated with NAC (0.1, 1, 10 μM) for 3 h at 37 °C. Parasite culture was then washed with PBS before the chemosensitivity assay. Parasite growth was determined spectrophotometrically (OD_{650}) by measuring the activity of the parasite lactate dehydrogenase (pLDH), according to a modified version of Makler's method in control and drug-treated cultures [38]. Antiplasmodial activity is expressed as the 50% inhibitory concentrations (IC_{50}) which is the dose of compound necessary to inhibit cell growth by 50%.

5.3.1. Combination of compound 9 with DHA

The *in vitro* interactions of compound **9** with DHA were determined by the analysis of the isobolograms. The drugs were applied alone or in combination against W2 strain of *Pf*. Five fixed doses of DHA (from 0.8 to 0.002 nM) were added to the dose-response curves of compound **9** (from the dose of 5 μM to 0.075 μM). In addition, a dose-response curve of DHA alone was performed to obtain the IC_{50} of DHA alone.

Isobolograms were constructed by plotting a pair of fractional IC_{50} s for each combination of compound **9** with DHA. The fractional IC_{50} for compound **9** was calculated by dividing the IC_{50} of compound **9** in combination with DHA by the IC_{50} of compound **9** alone and this data were plotted on the horizontal axis. The corresponding DHA fractional IC_{50} was calculated by dividing each fixed concentration by the IC_{50} of the DHA alone and was plotted on the vertical axis. An isobologram close to the diagonal indicates an additive effect. Curves above or below the diagonal indicate antagonistic or synergistic effect, respectively.

5.4. Cytotoxicity assay

The long-term human microvascular endothelial cell line (HMEC-1) was maintained in MCDB 131 medium (Invitrogen, Milan, Italy) supplemented with 10% heat-inactivated fetal calf serum (HyClone, Celbio,

Milan, Italy), 10 ng/ml of epidermal growth factor (Chemicon), 1 µg/ml of hydrocortisone, 2 mM glutamine, 100 U/ml of penicillin, 100 µg/ml of streptomycin, and 20 mM HEPES buffer (EuroClone). The human THP-1 monocytic leukaemia cells were maintained in RPMI 1640 (EuroClone) supplemented with 100 U/ml of penicillin, 100 µg/ml streptomycin, 20 mM HEPES, 1 mM Sodium Pyruvate, 0.05 mM β-mercaptoethanol, and 10% heat-inactivated fetal calf serum (EuroClone). The immortalized mouse C57Bl/6 bone marrow macrophages (BMDM) were maintained in DMEM, supplemented with 10% fetal calf serum (EuroClone), 25 mM HEPES, 4 mM L-glutamine, and 10 µg/ml ciprofloxacin.

For the cytotoxicity assays, cells were treated with serial dilutions of test compounds for 72 h and cell proliferation was evaluated using the MTT [39]. The results are expressed as IC₅₀.

5.5. Haemolysis and formation of methaemoglobin

Infected RBC, (iRBC, at 1–2% parasitemia) or fresh RBCs were diluted to 1% hematocrit in medium and incubated for 24 h with different doses of compounds 5 and 9 (from 59.5 to 0.9 µM). Haemolysis was evaluated by measuring spectrophotometrically the release of haemoglobin in the supernatants (absorbance at 405 nm, Soret band) and calculating the ratio of untreated to compounds-treated samples. The percentage of haemolysis for RBCs was determined by referring to a standard curve prepared with serially diluted RBCs lysed with saponin (1%).

To evaluate the formation of methaemoglobin, RBC were incubated in medium or in the presence of NAC (1–10 µM) for 3 h. RBC were then washed with PBS and incubated for 24 h at 37 °C with different doses of compound 5 and 9 (from 59.5 to 0.9 µM). At the end of the incubation, RBC were lysed and the percentage of oxyhaemoglobin or methaemoglobin was determined using the algorithm of Winterbourn based on the measurement of optical densities at 560, 577 and 630 nm [30].

5.6. Molecular modeling studies

Molecular modeling calculations were performed on E4 Server Twin 2 × Dual Xeon-5520, equipped with two nodes. Each node: 2 × Intel® Xeon® QuadCore E5520-2.26Ghz, 36 GB RAM. The molecular modeling graphics were carried out on a personal computer equipped with Intel (R) Core(TM) i7-4790 processor and SGI Octane 2 workstations.

5.6.1. Conformational property analysis

The apparent pK_a and clogD values of new thiazinoquinone compounds were calculated by using the ACD/Percepta software (ACD/Percepta, Advanced Chemistry Development, Inc., Toronto, ON, Canada, 2017, <http://www.acdlabs.com>). All compounds were considered neutral in all calculations performed as a consequence of the estimation of percentage of neutral/ionized forms computed at pH 7.4 (blood pH value), pH 7.2 (cytoplasm pH value), and 5.5 (Pf food vacuole pH), using the Handerson–Hasselbalch equation. Atomic potentials and charges were assigned using the CFF91 force field [40]. The conformational space of the compounds was sampled through 200 cycles of Simulated Annealing ($\epsilon = 80 \cdot r$). The following protocol was applied: the system was heated up to 1000 K over 2000 fs (time step = 3.0 fs); the temperature of 1000 K was applied to the system for 2000 fs (time step = 3.0 fs) with the aim of surmounting torsional barriers; successively, temperature was linearly reduced to 300 K in 1000 fs (time step = 1.0 fs). Resulting conformations were then subjected to molecular mechanic (MM) energy minimization within Insight 2005 Discover module (CFF91 force field; $\epsilon = 80 \cdot r$) until the maximum RMS derivative was less than 0.001 kcal/Å, using Conjugate Gradient [41] as minimization algorithm. Finally, the resulting conformers were ranked by their potential energy values (i.e., ΔE from the global energy minimum) and grouped into conformational sub-families on the basis of dihedral angle values (i.e., τ_1 and τ_2).

5.6.2. Redox property analysis

The lowest energy conformer of each sub-family of 4–5, 8–9 and 15 have been then subjected to DFT calculations. The calculations were carried out using the Gaussian 09 package [42]. All structures were fully optimized at the B3LYP/6–31 + G(d,p) level [43,44] using the conductor-like polarizable continuum model (C-PCM) [24]. The C-PCM method allows the calculation of the energy in the presence of a solvent. In this case all structures were optimized as a solute in an aqueous solution. In order to characterize every structure as minimum a vibrational analysis was carried out at the same level of theory using the keyword freq. The RMS force criterion was set to 3×10^{-4} a.u. Molecular orbitals and spin density have been calculated using the natural bond orbital (NBO) method [25]. Starting from the structure of the DFT Q (i.e., the starting quinone species) GM conformers, the redox states Q^{•-} and QH[•] were generated. In particular, following the reduction pathway of quinones showed in Scheme 3, each species was generated starting from the DFT optimized species of the previous step and submitted to full DFT optimization.

Finally, a fragment-based search in the Cambridge Crystallographic Structural Database (CSD) using the CSDS software Conquest 1.19 (Cambridge Structural Database System 2016) was performed in order to investigate which functional group of the methoxy-thiazinoquinone system could be suitable for iron interaction. In particular, the following fragments in complex with iron were used as probes: 1-methoxypropan-2-ol, 1-methoxypropan-2-one, 1-methoxyprop-1-en-2-ol, 3-methoxyprop-1-en-2-ol, 1-(methylamino)propan-2-ol, 1-(methylamino)propan-2-one, 1-(methylamino)prop-1-en-2-ol, 3-(methylamino)prop-1-en-2-ol, 1-(methylsulfonyl)propan-2-ol, 1-(methylsulfonyl)propan-2-one, 1-(methylsulfonyl)prop-1-en-2-ol, 3-(methylsulfonyl)prop-1-en-2-ol, and (methylsulfonyl)methane. The identified hits were analysed using the softwares Conquest 1.19 and Insight 2005 (Accelrys, San Diego, CA).

Author contributions

The manuscript was written through contributions of all authors. All authors have given approval to the final version of the manuscript.

Acknowledgment

This work was also supported by Ministero dell'Istruzione, dell'Università e della Ricerca (PRIN) Projects 2010C2LKKJ_006; 20154JRJPP_004. The authors acknowledge AVIS-Milano for providing fresh human blood for parasite cultures.

Appendix A. Supplementary material

Supplementary data to this article can be found online at <https://doi.org/10.1016/j.bioorg.2018.12.031>.

References

- [1] WHO, World malaria Report, < <http://www.who.int/malaria/publications/world-malaria-report-2017/report/en/> > .
- [2] C.J. Murray, L.C. Rosenfeld, S.S. Lim, K.G. Andrews, K.J. Foreman, D. Haring, N. Fullman, M. Naghavi, R. Lozano, A.D. Lopez, Global malaria mortality between 1980 and 2010: a systematic analysis, *Lancet* 379 (2012) 413–431.
- [3] M.A. Biamonte, J. Wanner, K.G. Le Roch, Recent advances in malaria drug discovery, *Bioorg. Med. Chem. Lett.* 23 (2013) 2829–2843.
- [4] E. Fattorusso, O. Tagliatalata-Scafati, Marine antimalarials, *Mar. Drugs* 7 (2009) 130–152.
- [5] C.F.C. Lam, A.N. Pearce, S.H. Tan, M. Kaiser, B.R. Copp, Discovery and evaluation of thiazinoquinones as anti-protozoal agents, *Mar. Drugs* 11 (2013) 3472–3499.
- [6] R.A. Davis, S. Duffy, S. Fletcher, V.M. Avery, R.J. Quinn, Thiaplakortones A-D: antimalarial thiazine alkaloids from the Australian marine sponge *Plakortis lita*, *J. Org. Chem.* 78 (2013) 9608–9613.
- [7] A. Aiello, E. Fattorusso, P. Luciano, A. Mangoni, M. Menna, Isolation and structure determination of aplidinones A-C from the Mediterranean ascidian *Aplidium conicum*: a successful regiochemistry assignment by quantum mechanical ¹³C NMR chemical shift calculations, *Eur. J. Org. Chem.* (2005) 5024–5030.

- [8] C. Imperatore, M. Persico, A. Aiello, P. Luciano, M. Guiso, M.F. Sanasi, D. Taramelli, S. Parapini, G. Cebrián-Torrejón, A. Doménech-Carbó, C. Fattorusso, M. Menna, Marine inspired antiplasmodial thiazinoquinones: synthesis, computational studies and electrochemical assays, *RSC Adv.* 5 (2015) 70689–70702.
- [9] A. Aiello, E. Fattorusso, P. Luciano, M. Menna, M.A. Calzado, E. Munoz, F. Bonadies, M. Guiso, M.F. Sanasi, G. Cocco, R. Nicoletti, Synthesis of structurally simplified analogues of aplidinone A, a pro-apoptotic marine thiazinoquinone, *Bioorg. Med. Chem.* 18 (2010) 719–727.
- [10] A. Aiello, E. Fattorusso, P. Luciano, A. Macho, M. Menna, E. Muñoz, Antitumor effects of two novel naturally occurring terpene quinones isolated from the Mediterranean ascidian *Aplidium conicum*, *J. Med. Chem.* 48 (2005) 3410–3416.
- [11] A. Aiello, E. Fattorusso, P. Luciano, M. Menna, G. Esposito, T. Iuvone, D. Pala, Conicaquinones A and B, two novel cytotoxic terpene quinones from the Mediterranean ascidian *Aplidium conicum*, *Eur. J. Org. Chem.* 5 (2003) 898–900.
- [12] M. Menna, A. Aiello, F. D'Aniello, C. Imperatore, P. Luciano, R. Vitalone, C. Itrace, R. Santamaria, Conithiaquinones A and B, tetracyclic cytotoxic meroterpenes from the Mediterranean ascidian *Aplidium conicum*, *Eur. J. Org. Chem.* 16 (2013) 3241–3246.
- [13] C. Imperatore, P. Cimino, G. Cebrián-Torrejón, M. Persico, A. Aiello, M. Senese, C. Fattorusso, M. Menna, A. Doménech-Carbó, Insight into the mechanism of action of marine cytotoxic thiazinoquinones, *Mar. Drugs* 15 (2017) 335.
- [14] S. Spyroudis, Hydroxyquinones: synthesis and reactivity, *Molecules* 5 (2000) 1291–1330.
- [15] A. Carbone, C.L. Lucas, C.J. Moody, Biomimetic synthesis of the apoptosis-inducing thiazinoquinone thiaplidiquinone A, *J. Org. Chem.* 77 (2012) 9179–9189.
- [16] A.N. Pearce, E.W. Chia, M.V. Berridge, G.R. Clark, J.L. Harper, L. Larsen, E.W. Maas, M.J. Page, N.B. Perry, V.L. Webb, B.R. Copp, Anti-inflammatory thiazine alkaloids isolated from the New Zealand ascidian *Aplidium* sp.: inhibitors of the neutrophil respiratory burst in a model of gouty arthritis, *J. Nat. Prod.* 70 (2007) 936–940.
- [17] C. Waterlot, D. Couturier, M. De Backer, B. Rigo, A study of hydrogenation of benzhydrols in the presence of catalytic amount of triflic acid, *Can. J. Chem.* 78 (2000) 1242–1246.
- [18] H. Mayr, B. Dogan, Selectivities in ionic reductions of alcohols and ketones with triethylsilane/trifluoroacetic acid, *Tetrahedron Lett.* 38 (1997) 1013–1016.
- [19] J.J. Kessl, N.V. Moskalev, G.W. Gribble, M. Nasr, S.R. Meshnick, B.L. Trumpower, Parameters determining the relative efficacy of hydroxy-naphthoquinone inhibitors of the cytochrome bc1 complex, *Biochim. Biophys. Acta* 1767 (2007) 319–326.
- [20] A. Saleh, J. Friesen, S. Baumeister, U. Gross, W. Bohne, Growth inhibition of *Toxoplasma gondii* and *Plasmodium falciparum* by nanomolar concentrations of 1-hydroxy-2-dodecyl-4(1H)quinolone, a high-affinity inhibitor of alternative (type II) NADH dehydrogenases, *Antimicrob. Agents Chemother.* 51 (2007) 1217–1222.
- [21] C.A. Lipinski, F. Lombardo, B.W. Dominy, P.J. Feeney, Experimental and computational approaches to estimate solubility and permeability in drug discovery and development settings, *Adv. Drug Deliv. Rev.* 46 (2001) 3–26.
- [22] D.P. Sonawane, M. Persico, Y. Corbett, G. Chianese, A. Di Dato, C. Fattorusso, O. Tagliatalata-Scafati, D. Taramelli, C. Trombini, D.D. Dhavale, A. Quintavalla, M. Lombardo, New antimalarial 3-methoxy-1,2-dioxanes: optimization of cellular pharmacokinetics and pharmacodynamics properties by incorporation of amino and N-heterocyclic moieties at C4, *RSC Adv.* 5 (2015) 72995–73010.
- [23] K. Kirk, Membrane transport in the malaria-infected erythrocyte, *Physiol. Rev.* 81 (2001) 495–537.
- [24] M. Cossi, N. Rega, G. Scalmani, V. Barone, Energies, structures, and electronic properties of molecules in solution with the C-PCM solvation model, *J. Comp. Chem.* 24 (2003) 669–681.
- [25] A.E. Reed, R.B. Weinstock, F. Weinhold, Natural population analysis, *J. Chem. Phys.* 83 (1985) 735–746.
- [26] P.A. Sigala, D.E. Goldberg, The peculiarities and paradoxes of *Plasmodium* heme metabolism, *Annu. Rev. Microbiol.* 68 (2014) 259–278.
- [27] J. Wang, C.J. Zhang, W.N. Chia, C.C. Loh, Z. Li, Y.M. Lee, Y. He, L.X. Yuan, T.K. Lim, M. Liu, C.X. Liew, Y.Q. Lee, J. Zhang, N. Lu, C.T. Lim, Z.C. Hua, B. Liu, H.M. Shen, K.S. Tan, Q. Lin, Haem-activated promiscuous targeting of artemisinin in *Plasmodium falciparum*, *Nat. Commun.* 6 (2015) 10111.
- [28] I. Elbini Dhoubi, M. Jallouli, A. Annabi, N. Gharbi, S. Elfazaa, M.M. Lasram, A minireview on N-acetylcysteine: an old drug with new approaches, *Life Sci.* 151 (2016) 359–363.
- [29] P. Arreesrisom, A.M. Dondorp, S. Looareesuwan, R. Udomsangpetch, Suppressive effects of the anti-oxidant N-acetylcysteine on the anti-malarial activity of artesunate, *Parasitol. Int.* 56 (2007) 221–226.
- [30] J. Szebeni, C.C. Winterbourn, R.W. Carrell, Oxidative interactions between hemoglobin and membrane lipid. A liposome model, *Biochem. J.* 220 (1984) 685–692.
- [31] K.H. Taber, P.J. Migliore, J.J. Pagani, J.J. Ford, T. McLauren, L.A. Hayman, Temporal changes in the oxidation state in vitro blood, *Invest Radiol.* 25 (1990) 240–244.
- [32] B.T. Mott, R.T. Eastman, R. Guha, K.S. Sherlach, A. Siritwardana, P. Shinn, C. McKnight, S. Michael, N. Lacerda-Queiroz, P.R. Patel, P. Khine, H. Sun, M. Kasbekar, N. Aghdam, S.D. Fontaine, D. Liu, T. Mierzwa, L.A. Mathews-Griner, M. Ferrer, A.R. Renslo, J. Inglese, J. Yuan, P.D. Roepe, X.Z. Su, C.J. Thomas, High-throughput matrix screening identifies synergistic and antagonistic antimalarial drug combinations, *Sci. Rep.* 5 (2015) 13891.
- [33] O. Tagliatalata-Scafati, E. Fattorusso, A. Romano, F. Scala, V. Barone, P. Cimino, E. Stendardo, B. Catalanotti, M. Persico, C. Fattorusso, Insight into the mechanism of action of plakortins, simple 1,2-dioxane antimalarials, *Org. Biomol. Chem.* 8 (2010) 846–856.
- [34] S. Kamchonwongpaisan, S.R. Meshnick, The mode of action of the antimalarial artemisinin and its derivatives, *Gen. Pharmac.* 27 (1996) 587–592.
- [35] C.L. Peatey, D. Leroy, D.L. Gardiner, K.R. Trenholme, Anti-malarial drugs: how effective are they against *Plasmodium falciparum* gametocytes? *Malar. J.* 11 (2012) 34.
- [36] A.S. Butterworth, T.S. Skinner-Adams, D.L. Gardiner, K.R. Trenholme, *Plasmodium falciparum* gametocytes: with a view to a kill, *Parasitology* 140 (2013) 1718–1734.
- [37] G. Chianese, M. Persico, F. Yang, H.W. Lin, Y.W. Guo, N. Basilico, S. Parapini, D. Taramelli, O. Tagliatalata-Scafati, C. Fattorusso, Endoperoxide polyketides from a Chinese *Plakortis simplex*: further evidence of the impact of stereochemistry on antimalarial activity of simple 1,2-dioxanes, *Bioorg. Med. Chem.* 22 (2014) 4572–4580.
- [38] M.T. Makler, J.M. Ries, J.A. Williams, J.E. Bancro, R.C. Piper, B.L. Gibbins, D.J. Hinrichs, Parasite lactate dehydrogenase as an assay for *Plasmodium falciparum* drug sensitivity, *Am. J. Trop. Med. Hyg.* 48 (1993) 739–741.
- [39] T. Mosmann, Rapid colorimetric assay for cellular growth and survival: application to proliferation and cytotoxicity assays, *J. Immunol. Methods* 65 (1983) 55–63.
- [40] J.R. Maple, M.J. Hwang, T.P. Stockfisch, U. Dinur, M. Waldman, C.S. Ewig, A.T. Hagler, Derivation of class II force fields: I. Methodology and quantum force field for the alkyl functional group and alkane molecules, *J. Comput. Chem.* 15 (1994) 162–182.
- [41] R. Fletcher, Unconstrained optimization, *Practical Methods of Optimization* vol. 1, (1980).
- [42] M.J. Frisch, G.W. Trucks, H.B. Schlegel, G.E. Scuseria, M.A. Robb, J.R. Cheeseman, G. Scalmani, V. Barone, B. Mennucci, G.A. Petersson, H. Nakatsuji, M. Caricato, X. Li, H.P. Hratchian, A.F. Izmaylov, J. Bloino, G. Zheng, J.L. Sonnenberg, M. Hada, M. Ehara, K. Toyota, R. Fukuda, J. Hasegawa, M. Ishida, T. Nakajima, Y. Honda, O. Kitao, H. Nakai, T. Vreven, J.A. Jr, J.E. Montgomery, F. Peralta, M. Ogliaro, J.J. Bearpark, E. Heyd, K.N. Brothers, V.N. Kudin, R. Staroverov, J. Kobayashi, K. Normand, A. Raghavachari, J.C. Rendell, S.S. Burant, J. Iyengar, M. Tomasi, N. Cossi, N.J. Rega, M. Millam, J.E. Klene, J.B. Knox, V. Cross, C. Bakken, J. Adamo, R. Jaramillo, R.E. Gomperts, O. Stratmann, A.J. Yazyev, R. Austin, C. Cammi, J.W. Pomelli, R.L. Chterski, K. Martin, V.G. Morokuma, G.A. Zakrzewski, P. Voth, J.J. Salvador, S. Dannenberg, A.D. Dapprich, O. Daniels, J.B. Farkas, J.V. Foresman, J. Ortiz, D.J. Fox Cioslowski, Gaussian 09, revision A.1, Gaussian Inc., Wallingford, 2009.
- [43] M.D. Becke, Density-functional thermochemistry. III. The role of exact exchange, *J. Chem. Phys.* 98 (1993) 5648–5652.
- [44] C. Lee, W. Yang, R.G. Parr, Development of the Colle-Salvetti correlation-energy formula into a functional of the electron density, *Phys. Rev. B: Condens. Matter Phys.* 37 (1988) 785–789.